Effect of elastic anisotropy on the elastic fields and vertical alignment of quantum dots

Q. X. Pei, [a] C. Lu, and Y. Y. Wang
Institute of High Performance Computing, 1 Science Park Road, Singapore 117528, Singapore

(Received 24 June 2002; accepted 13 November 2002)

The elastic fields in the self-organized quantum dot (QD) structures are investigated in details by three-dimensional finite element analysis for an array of lens shaped QDs. Emphasis is placed on the effect of elastic anisotropy of the materials with the anisotropy ratio A ranging from 0.25 to 4.0 for both the QDs and the matrix. It is found that the elastic anisotropy strongly influences the distributions of strain, stress, and strain energy density in the QD structures. It is shown that the elastic interactions among the buried QDs play crucial role in the formation of the satellite energy minima at the cap layer surface, while the materials anisotropy and the cap layer thickness also play important roles. By changing the elastic anisotropy ratio and the cap layer thickness, substantially different distributions of strain energy minima on the cap layer surface are obtained, which may result in various QD ordering phenomena such as vertical alignment, partial alignment, or complete misalignment. Based on the calculation results, a phase diagram is constructed to show the effect of material anisotropy and cap layer thickness on the vertical correlation of QDs. © *2003 American Institute of Physics.* [DOI: 10.1063/1.1535730]

I. INTRODUCTION

Quantum dots (QDs) have drawn great attention due to their potential application in the fabrication of a wide variety of optoelectronic and microelectronic devices, such as light emitting diodes, photovoltaic cells, and quantum semiconductor lasers.[1,2] Self-assembled QDs can be grown layer by layer to form ordered nanostructures via the Stranski–Krastanow growth mode that consists of three-dimensional (3D) inlands growth on a two-dimensional (2D) wetting layer. It is well understood that such self-alignment is due to long-range elastic fields induced by the misfit strain between the QDs and the substrate.[3,4] It is also well known that the elastic fields produced by the QDs substantially modify the electronic band structure and so strongly affect the performance of the electronic devices.[5] Hence, the elastic fields in and around the QDs have to be studied in order to obtain a well ordered QD structure and improve the performance of the electronic devices.

The elastic fields in and around the QDs have recently been analyzed by many researchers using a variety of techniques such as atomistic approach,[6–9] analytical continuum approach,[10–14] and finite element approach.[15–17] The atomistic approach is based on the ball and spring models and describes the strain energy in terms of few-body potentials between the atoms. The strain fields are obtained by minimizing the strain energy. The empirical potentials or the quantum-mechanical Schrödinger equation is used in the calculations. Because a large number of atoms is required in the analysis, this approach is computationally intensive and is now limited to a single QD. In the analytical continuum approach, the QDs are treated as inclusions in a matrix. The elastic fields due to the lattice mismatch between the QDs and the matrix are obtained by integrating the Green's function over the volume of the inclusions. However, the integration can only be done for some simple inclusion shapes, such as cuboid, pyramid, and truncated pyramid. In the finite element approach, the finite element method (FEM) is used to determine the strain and stress distributions in the QD structure. Comparing to the other two approaches, the FEM technique is more powerful and can be used for structures of any geometry shape.

From the survey of the literatures on the elastic fields in QDs, it is found that at least one or more of the following simplifications have been made in the calculations.

(1) Dealing with a single isolated QD. This simplification has been used by many researchers, especially those utilizing the atomistic approach. However, this simplification ignores the elastic interactions among multiple QDs.

(2) Assuming an infinite matrix. Although QDs are buried under free surface, most of the analyses with the analytical continuum approach are made with the QD buried in an infinite matrix.

(3) Using a simple geometry of QD. Some simple QD geometries are used, such as 2D axisymmetric model of conical shape, 3D models of cuboid, pyramid, and truncated pyramid shapes. However, the typical shape of QDs is lens shape, because it is most widely observed in experiments and is believed to be the final phase of QD shape transition.[18,19] Since it is more difficult to model lens shape than other simple shapes, no calculation of the elastic fields induced by lens shaped QDs has been reported.

(4) Excluding the wetting layer. Most of the calculations are made without the wetting layer. As the wetting layer is the misfit strain transition layer between the QDs and the matrix, it is obvious that its existence will have some influence on the elastic fields in and around the QDs.

[a]Electronic mail: peiqx@ihpc.a-star.edu.sg

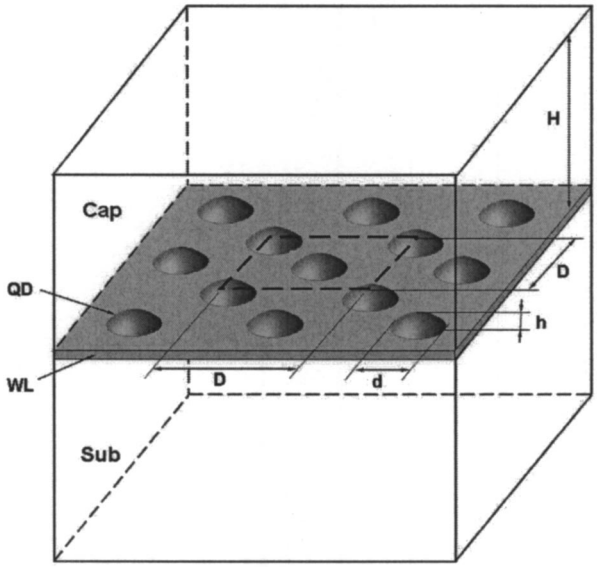

FIG. 1. Schematic of an array of lens shaped QDs. The islands with height of h are formed on the WL deposited on the substrate. The islands are subsequently covered with the cap layer. Due to symmetry, the analysis region is chosen to be the central square area surrounded by the heavy dotted lines.

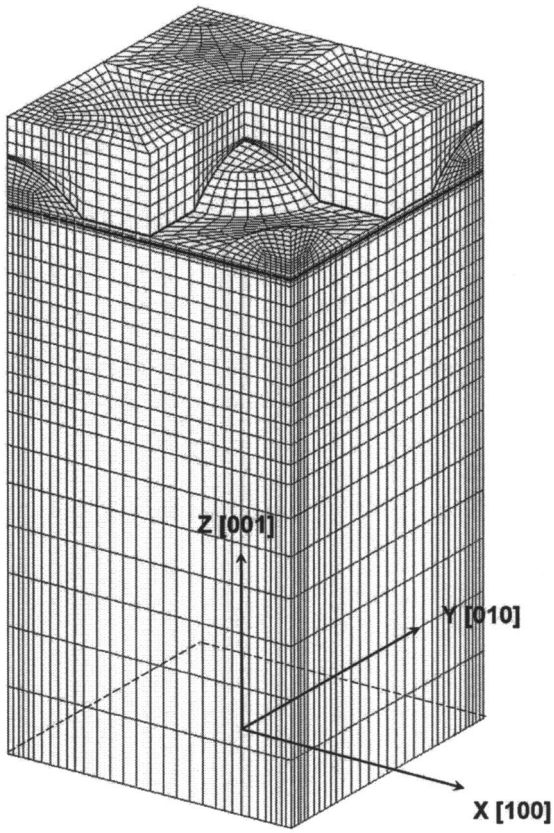

FIG. 2. The finite element mesh used in the analysis. Part of the cap layer mesh is removed to show the mesh of the central QD. The origin of the coordinate system is located at the center of the bottom surface of the model.

(5) Assuming isotropic materials. In most of the existing works, the isotropic elasticity of materials is assumed for both the QDs and the matrix. Although the anisotropic elasticity effect is studied by some researchers,[14,20] either a single point strain source or an isolated QD is assumed in their analyses. Until now, report on detailed study of the elastic anisotropy effect on the elastic fields has not been found for a multiple QD system.

Some of the most recent works in this area are: Glas[13] analyzed the strain fields induced by a single truncated pyramidal QD buried in a half space using the analytical approach with the isotropic elasticity. Makeev *et al.*[9] studied the dependence of the cap layer surface stress on the island volume and the cap layer thickness with the atomistic simulation of a pyramidal QD. Romanov *et al.*[16] studied the stress distribution at the top surface of the cap layer for a array of QDs buried at different depths. The dot geometries were approximated as oblate spheroids with the analytical solution and as cuboids and truncated pyramids with the FEM approach. The isotropic elasticity was assumed and the wetting later was not included in their analysis. Pan *et al.*[14] calculated the elastic fields in an anisotropic matrix using the analytical approach. However, only an isolated cubic QD without wetting layer was used in their model.

In this article, we report on a three-dimensional FEM calculation of the elastic fields induced by an array of lens shaped QDs with wetting layer, which are submerged in a semi-infinite half space. We present a detailed study of materials anisotropy effects on the elastic fields in the multiple QD system and on the vertical ordering of the QDs.

II. ANALYSIS METHOD AND CONDITIONS

A schematic of the lens shaped QD array is shown in Fig. 1, assuming the QDs are distributed uniformly. Due to symmetry of the structure we only analyze the central square area surrounded by the heavy dotted lines, which covers one complete QD and four quarter QDs. In the model, the distance (D) between the two side QDs is taken to be 45 nm, while the thickness of the wetting layer (WL) is taken to be 1 nm. The base diameter (d) of the lens shaped QD is taken to be 24 nm with its height (h) being 6 nm.

The 3D finite element model using MSC/MARC, a commercial FEM code, is shown in Fig. 2. The symmetry boundary conditions are applied at the four side faces, while the fixed displacement boundary conditions are imposed at the bottom surface of the model. The substrate thickness is taken to be 80 nm, which is shown to be big enough for the bottom surface to be considered as ''far field,'' so that the defined boundary conditions at the bottom surface have little influence on the FEM results. The origin of the coordinate system is located at the center of the bottom surface. The Z [001] direction points upwards, which means the QDs are grown on the (001) surface of the substrate. The QD lattice constant a_d is taken to be bigger than the matrix lattice constant a_m with the lattice misfit $\varepsilon_0=(a_d-a_m)/a_m=0.04$. This lattice mismatch is modeled by employing a pseudothermal expansion of the QDs. A thermal expansion coefficient of 0.04 is applied in the finite elements of the QDs and the wetting layer, while the temperature is raised by 1 K. This forms the strain load in the FEM model. For materials of cubic crys-

TABLE I. The anisotropy ratio and the corresponding elastic constants.

A	C_{11} (GPa)	C_{12} (GPa)	C_{44} (GPa)
1.0	150	50	50
0.25	150	50	12.5
0.5	150	50	25
2.0	150	50	100
4.0	150	50	200

tals, the degree of elastic anisotropy is usually characterized by the anisotropy ratio $A=2C_{44}/(C_{11}-C_{12})$ with $A=1.0$ being isotropic elasticity. It is roughly equal to the ratio between the values of Young's modulus along the $<111>$ and the $<100>$ directions.[20] The A values for some semiconductor materials are: PbTe 0.27, PbSe 0.29, PbS 0.51, Si 1.56, Ge 1.64, GaAs 1.83, InAs 2.08, ZnTe 2.04, and ZnS 2.53. To cover most of the semiconductor materials, A values are taken in the range of 0.25–4.0 in our investigation. The elastic constants $C_{11}=150$, $C_{12}=50$, $C_{44}=50$ GPa are used for the elastic isotropy case $A=1.0$, while for each of the four elastic anisotropy cases $A=0.25$, 0.5, 2.0, and 4.0, C_{11} and C_{12} are kept unchanged with C_{44} adjusted to make A equal to the corresponding value. The calculation cases with different A values and the corresponding elastic constants C_{11}, C_{12}, and C_{44} are shown in Table I.

The A values of the QDs and the matrix can be different in our FEM model, however, we use the same A value for the QDs and the matrix in each calculation case in order to see the effects of elastic anisotropy more clearly. This treatment is also due to the fact that the A values of the QDs and the matrix are very close in each of the commonly observed QD structures such as Ge/Si, InAs/GaAs, and PbSe/PbTe.

Calculations are also carried out for different cap layer thickness with the ratio of cap layer thickness to dot height, H/h, being 2.0, 3.0, 4.0, 5.0, and 6.0, respectively.

III. RESULTS AND DISCUSSION

A. Strain and stress distributions

We now analyze the calculation results with the cap layer thickness $H/h=2.0$. Figure 3(a) shows the contour plot of the strain ε_{xx} distribution in the $Y=0$ plane for the case of elastic isotropy $A=1$. Due to the lattice parameter of the QD and the wetting layer being larger than that of the matrix, it can be seen that negative ε_{xx}, i.e., compressive strain, occurs in the QD and the wetting layer. In the matrix, positive ε_{xx}, i.e., tensile strain, occurs in the regions directly below and above the QD, while small compressive strain exists in the regions near the QD corners. These ε_{xx} distributions bear some similar characteristics to the analytical results of Glas[13] with truncated pyramid QD assuming isotropic elasticity. However, there are some differences in ε_{xx} distributions between the two island shapes. One of them is that the maximum strain relaxation occurs at the top of the lens shaped QD, while it occurs at the up corners of the truncated pyramid QD. This clearly shows that the island shape has great influence on the strain field.

The influence of elastic anisotropy on ε_{xx} distributions in the $Y=0$ plane is shown in Figs. 3(b)–3(e) for the cases

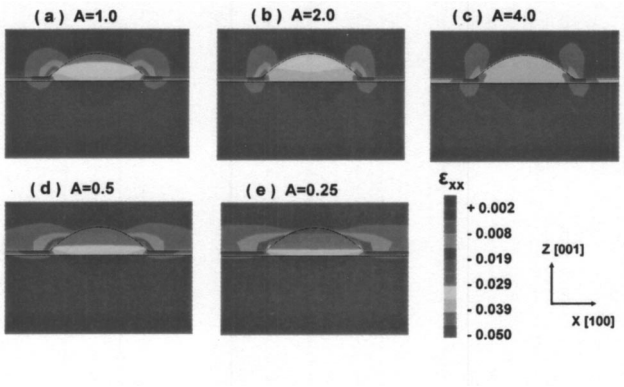

FIG. 3. The strain ε_{xx} distributions in the $Y=0$ plane for different values of anisotropy ratio A. (a) $A=1.0$, (b) $A=2.0$, (c) $A=4.0$, (d) $A=0.5$, and (e) $A=0.25$. The effect of elastic anisotropy on ε_{xx} can be clearly seen from the contour maps.

with the elastic anisotropy ratio $A=2.0$, 4.0, 0.5, and 0.25, respectively. Significant difference of ε_{xx} distributions can be observed in these maps. In the QD, the value of ε_{xx} contour increases with A changing from 1.0 to 4.0, while it decreases with A changing from 1.0 to 0.25. In the matrix around the QD corners, the ε_{xx} contour shapes are more horizontally narrowed with A increasing, while they become more horizontally elongated with A decreasing. This clearly shows that when $A>1$, the [100] and the $[\bar{1}00]$ directions are the elastically soft directions and thus the strain ε_{xx} decays rapidly in these directions. When $A<1$, the [100] and the $[\bar{1}00]$ directions are elastically hard directions and thus the strained region extends further away along these directions.

Figures 4(a) and 4(b) show the effect of elastic anisotropy on the strain profiles of ε_{xx} and ε_{zz} along the line in the z direction through the QD center. For the various A values, ε_{xx} is positive in the matrix and gradually increases from near zero to the local maximum at the interface between the matrix and the wetting layer. ε_{xx} changes its sign to negative in the QD region and its absolute value reduces as it reaches the interface between the QD and the cap layer. In the cap layer region, ε_{xx} changes its sign back to positive. Although the overall shapes of ε_{xx} profiles are similar for different A values, there are also big differences between them. As A increases from 0.25 to 4.0, the compressive strain in the QD increases considerably, while the tensile strain in the cap layer changes its profile too. The elastic anisotropy also has strong influence on ε_{zz} profile. As A increases from 0.25 to 4.0, the magnitude of ε_{zz} increases in the matrix while it decreases in the QD. When A increases to 4.0, compressive ε_{zz} and tensile ε_{zz} coexist in both the substrate and the QD.

The stress σ_v (von Mises) distributions at the $Y=0$ plane for the various A values are shown in Figs. 5(a)–5(e). It can be seen that high stress exists in the QD and in the matrix near the QD. The elastic anisotropy also has strong influence on the stress distributions: the stress contours change remarkably as A changes from 0.25 to 4.0, especially in the QD and in the matrix around the QD.

The effect of the cap layer thickness on the elastic fields is more obviously reflected by the strain energy density at the cap layer surface and is analyzed in the following section.

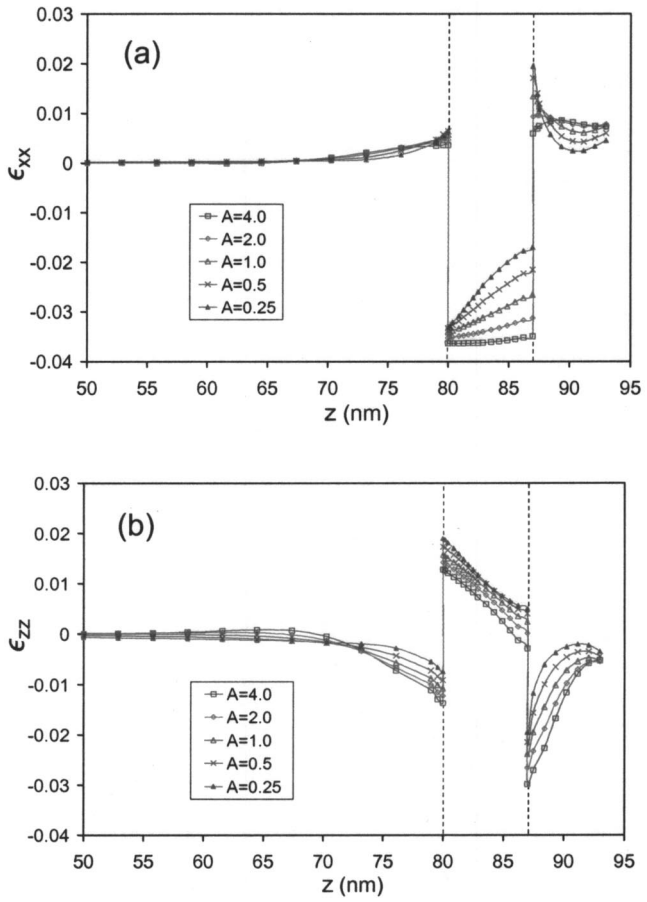

FIG. 4. Strain profiles along the line in the z direction through the QD center for different values of anisotropy ratio A. (a) ε_{xx} profiles. (b) ε_{zz} profiles. Dashed vertical lines show the positions of the interfaces between the substrate and the wetting layer and between the QD and the cap layer.

B. Strain energy density distribution and vertical alignment of QDs

In addition to analyzing the strain and stress distributions, another important purpose of calculating the elastic fields of QDs structures is to derive the QDs ordering conditions, if more than one layer is deposited. Experiments have shown that the top islands can be fully or partially aligned vertically, or completely misaligned with respect to the buried islands.[21–23] It has been found that the distribution of the strain energy density on the surface of the cap layer can provide very important information on the alignment of surface QDs with the buried QDs.[20,24–26] To be consistent with previous works,[12,20] the strain energy density E_S is evaluated using the following expression:

$$E_S = -\frac{1}{2}\sigma_{ij}\varepsilon_{ij}.$$

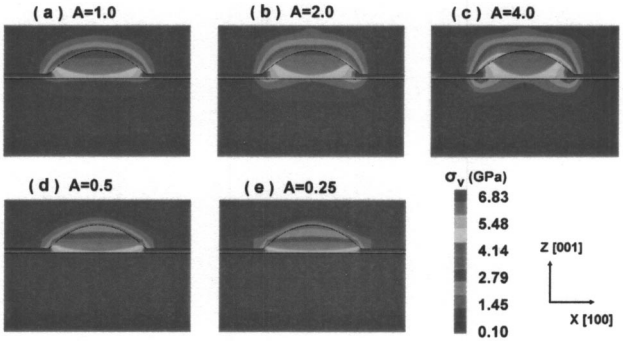

FIG. 5. The von Mises stress σ_v distributions in the $Y=0$ plane for different values of anisotropy ratio A. (a) $A=1.0$, (b) $A=2.0$, (c) $A=4.0$, (d) $A=0.5$, and (e) $A=0.25$. The effect of elastic anisotropy on σ_v can be clearly seen from the contour maps.

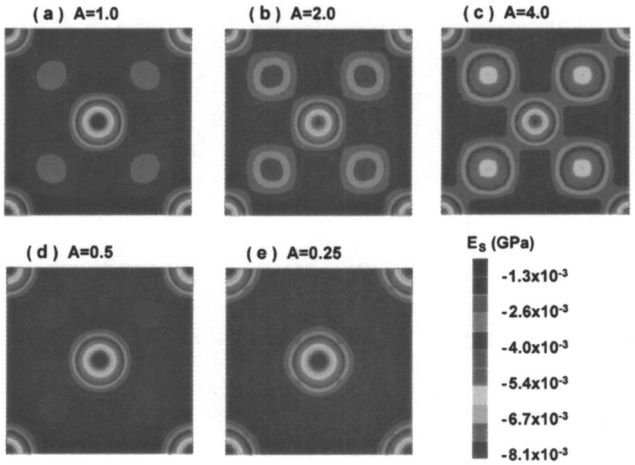

FIG. 6. The influence of elastic anisotropy on the distributions of strain energy density E_S on the surface of cap layer for the cap layer thickness $H/h=2.0$. (a) $A=1.0$, (b) $A=2.0$, (c) $A=4.0$, (d) $A=0.5$, and (e) $A=0.25$.

Figure 6(a) shows the distributions of strain energy density on the cap layer surface for the case of elastic isotropy $A=1$ and the cap layer thickness $H/h=2.0$. It can be seen that there are pronounced energy minima at positions directly above the buried QDs. These energy minima may make the QDs of the next layer to nucleate there preferentially, which result in vertical alignment of newly formed QDs with the buried QDs. It can also be seen in Fig. 6(a) that small satellite energy minima exist in the midway between the buried QDs. Satellite minima were also found by Jogai[12] with two or four closed spaced pyramid QDs. However, satellite minima cannot be observed in some researchers' results with a point strain source[20] or with an isolated QD.[14,17] We also made calculations with only one isolated QD and the satellite minima were not found. These results show that the elastic interaction between QDs is very important to the distribution of the energy minima on the cap layer surface.

Figures 6(b)–6(e) show the distributions of strain energy density on the cap layer surface for the anisotropy cases $A=2.0$, 4.0, 0.5, and 0.25, respectively. As A increases from 1.0 to 2.0 and further to 4.0, these satellite minima become more and more obvious. The depth of the satellite minima increases from about 25% of the pronounced minima in Fig. 6(a) to about 40% of the pronounced minima in Fig. 6(b) and further to about 70% of the pronounced minima in Fig. 6(c). Here we define that when the satellite minima are deeper

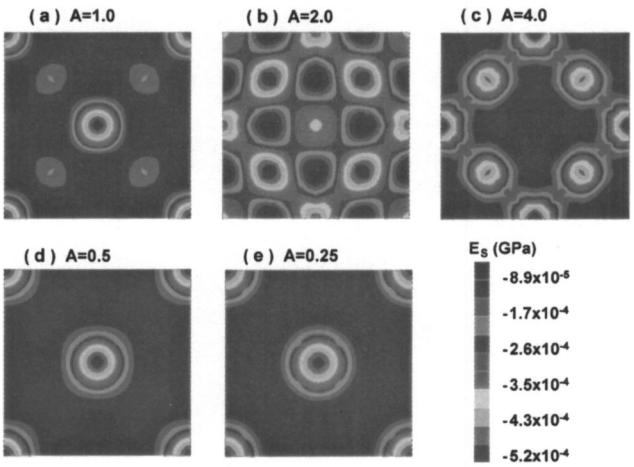

FIG. 7. The influence of elastic anisotropy on the distributions of strain energy density E_S on the surface of cap layer for the cap layer thickness $H/h=3.0$. (a) $A=1.0$, (b) $A=2.0$, (c) $A=4.0$, (d) $A=0.5$, and (e) $A=0.25$.

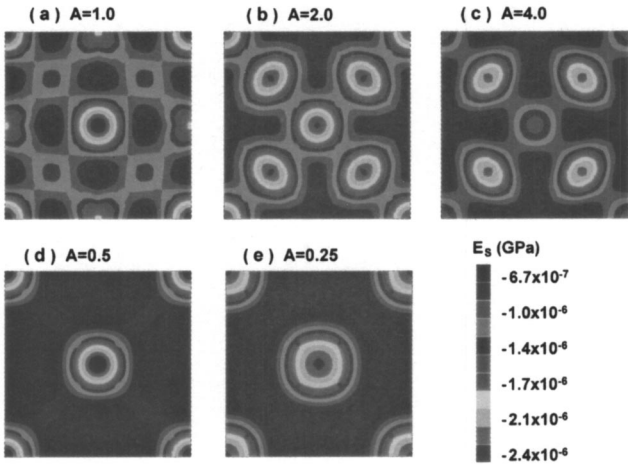

FIG. 8. The influence of elastic anisotropy on the distributions of strain energy density E_S on the surface of cap layer for the cap layer thickness $H/h=5.0$. (a) $A=1.0$, (b) $A=2.0$, (c) $A=4.0$, (d) $A=0.5$, and (e) $A=0.25$.

than 50% of the pronounced minima, the satellite minima have developed into local minima, which may lead to additional QDs formation in the next layer. Thus, in the situation of Fig. 6(c), some newly formed QDs may be misaligned vertically with the buried QDs. However, as A reduces from 1.0 to 0.5 and further to 0.25, the satellite minima become less obvious and gradually disappear and only the pronounced local minima at the top of the QDs remain as seen in Figs. 6(d) and 6(e), which may result in a fully vertically aligned QD structure.

When the cap layer thickness is increased to $H/h=3.0$, the strain energy distributions on the cap layer surface are shown in Figs. 7(a)–7(e). For the elastic isotropy case $A=1.0$, it can be seen in Fig. 7(a) that besides the pronounced local energy minima at positions directly above the QDs, there are some satellite minima at positions between the QDs. As A increases from 1.0 to 2.0, these satellite minima develop into pronounced local minima as seen in Fig. 7(b), which may result in a partially misaligned QD structure. As A increases further to 4.0, the original pronounced local minima above the QDs disappear and only the local minima between the QDs remain as seen in Fig. 7(c). In this situation, a totally misaligned (anticorrelated) structure may be formed. As A reduces from 1.0 to 0.5 and further to 0.25, it can be seen from Figs. 7(d) and 7(e) that the satellite minima disappear and only the pronounced local minima at the top of the QDs remain, which may result in a vertically aligned QDs structure.

When the cap layer thickness is further increased to $H/h=5.0$, the strain energy distributions on the cap layer surface are shown in Figs. 8(a)–8(e). For the elastic isotropy case $A=1.0$, it can be seen in Fig. 8(a) that there are pronounced local minima above and between the QDs, which may result in a partially aligned QD structure. As A increases from 1.0 to 2.0, the original satellite minima become pronounced local minima, while some of the original pronounced local minima disappear as seen in Fig. 8(b). In this situation, a partially aligned QD structure is favorable. As A increases further to 4.0, the original pronounced local minima above the QDs become almost disappeared and only the pronounced local minima between the QDs remain as seen in Fig. 8(c). In this situation, a completely misaligned structure may be formed. As A reduces from 1.0 to 0.5 and further to 0.25, it can be seen in Figs. 8(d) and 8(e) that the original local minima and satellite minima between the QDs disappear and only the pronounced local minima above the QDs remain, which may result in a vertically aligned structure.

Similar results are also obtained for the cap layer thickness $H/h=4.0$ and $H/h=6.0$. All the calculation results regarding the vertical alignment of QDs are listed in Table II. Based on the results, a phase diagram showing the vertical correlation of QDs grown on the (001) surface is constructed as shown in Fig. 9. In this diagram, there are two regions representing two differently ordered QD phases. In region I, the top QDs are vertically aligned with the buried QDs. In region II, the top QDs are partially aligned or completely misaligned with the buried QDs. From this diagram we can obtain the QDs ordering tendency according to the materials anisotropy A and the cap layer thickness H/h. For example, when H/h is more than 2.0, the vertical alignment may become partial alignment or complete misalignment with the increase of A. When A is smaller than 0.5, the vertical alignment is favorable even with thick cap layer. However, when H/h is larger than 6.0, the QDs will gradually lose vertical correlation, which is observed in experiments.[21–23]

The earlier calculation results and the phase diagram are based on the model with the QDs grown on the (001) surface. When the QDs are grown on the (111) surface, for the case of elastic isotropy $A=1$, there will be no difference between the FEM results of the QDs grown on the (111) surface and that of the QDs grown on the (001) surface. For the cases of elastic anisotropy, because A is roughly equal to the ratio between the values of Young's modulus along the [111] and the [001] directions, the calculation results of QDs grown on (111) surface with $A=C$ will be roughly the same

TABLE II. Calculated results of QD alignment. "O" represents fully vertical alignment, "X" represents partially alignment or completely misalignment

	Cap layer thickness H/h				
Anisotropy ratio A	2.0	3.0	4.0	5.0	6.0
4.0	X	X	X	X	X
2.0	O	X	X	X	X
1.0	O	O	X	X	X
0.5	O	O	O	O	O
0.25	O	O	O	O	O

to the results of QDs grown on (001) surface with $A=1/C$. Therefore, the phase diagram in Fig. 9 can also be used to obtain the QDs ordering tendency for the QDs grown on the (111) surface by using the reciprocal value of the QDs anisotropy ratio.

The predicted transitions between vertical alignment and misalignment have found supports from the experiments of Kienzle *et al.*[22] with Ge/Si(001), and Springholz *et al.*[23] with PbSe/PbEuTe(111) QDs structures. In the Kienzle's results, when H/h is more than 3.0, the QDs gradually lose vertical alignment and partially aligned or completely misaligned structures are obtained. This is in good agreement with the prediction from the phase diagram in Fig. 9 by using the average value of the anisotropy ratios of Ge and Si. In the Springholz's results, when H/h is more than 2.0, the arrangement of the QDs changes from vertical alignment to partial alignment or total misalignment. This is also in good agreement with the prediction from Fig. 9 by using the reciprocal value of the average anisotropy ratios of PbSe and PbEuTe.

The agreement with experimental results shows that the phase diagram has some practical meaning. Further works will be done regarding the influence of QDs geometry and spacing on the phase diagram.

IV. CONCLUSIONS

The three-dimensional finite element approach is used to calculate the elastic fields induced by an array of lens shape QDs buried in a matrix. The effects of elastic anisotropy of the materials on the elastic fields are investigated in details. It is found that the elastic anisotropy has significant influence on the elastic fields. Therefore, in calculating the elastic fields of QDs structure, the isotropy approximation should not be used, especially when the material exhibits strong anisotropy. It is also found that the elastic interactions among the buried QDs have strong influence on the strain energy distributions at the cap layer surface, which may result in vertical ordering of the surface QDs. Thus, a single strain source model or an isolated QD model ignoring the elastic interactions is not efficient to study the vertical ordering phenomena in structures with horizontally closed-spaced QDs. Our calculation results also show that the elastic anisotropy and the cap layer thickness have strong influence on the distribution of the energy minima at the cap layer surface. The phase diagram obtained from the present study clearly shows the various QDs ordering phenomena such as vertical alignment, partial alignment, or complete misalignment (vertical anticorrelation). The phase diagram has found some supports from experiments and it may be helpful to predict the QD ordering in future QD growth experiments.

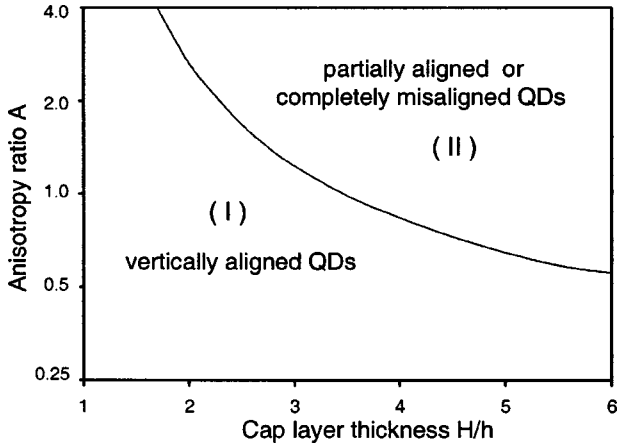

FIG. 9. Phase diagram showing the effects of elastic anisotropy and the cap layer thickness on the vertical correlation of QDs.

ACKNOWLEDGMENTS

The authors would like to thank Dr. Y. W. Zhang for helpful comments and Dr. F. Wang for proofreading the manuscript.

[1] J. Tersoff, C. Teichert, and M. G. Lagally, Phys. Rev. Lett. **76**, 1675 (1996).
[2] D. Bimberg, Semiconductors **33**, 951 (1999).
[3] V. A. Shchukin and D. Bimberg, Rev. Mod. Phys. **71**, 1125 (1999).
[4] Z. Suo and Z. Zhang, Phys. Rev. B **58**, 5116 (1998).
[5] O. G. Schmidt, K. Eberl, and Y. Rau, Phys. Rev. B **62**, 16 715 (2000).
[6] C. Pryor, J. Kim, L. W. Wang, A. J. Williamson, and A. Zunger, J. Appl. Phys. **83**, 2548 (1998).
[7] M. Califano and P. Harrison, Phys. Rev. B **61**, 10 959 (2000).
[8] Y. Kikuchi, H. Sugii, and K. Shintani, J. Appl. Phys. **89**, 1191 (2001).
[9] M. A. Makeev and A. Madhukar, Phys. Rev. Lett. **86**, 5542 (2001).
[10] A. D. Andreev, J. R. Downes, D. A. Faux, and E. P. O'Reilly, J. Appl. Phys. **86**, 297 (1999).
[11] G. S. Pearson and D. A. Faux, J. Appl. Phys. **88**, 730 (2000).
[12] B. Jogai, J. Appl. Phys. **88**, 5050 (2000).
[13] F. Glas, J. Appl. Phys. **90**, 3232 (2001).
[14] E. Pan and B. Yang, J. Appl. Phys. **90**, 6190 (2001).
[15] T. Benabbas, Y. Androussi, and A. Lefebvre, J. Appl. Phys. **86**, 1964 (1999).
[16] A. E. Romanov, G. E. Beltz, W. T. Fischer, P. M. Petroff, and J. S. Speck, J. Appl. Phys. **89**, 4523 (2001).
[17] G. R. Liu and S. S. Quek Jerry, Semicond. Sci. Technol. **17**, 630 (2002).
[18] F. M. Ross, R. M. Tromp, and M. C. Reuter, Science **286**, 1931 (1999).
[19] A. Rastelli, M. Kummer, and H. von Kanel, Phys. Rev. Lett. **87**, 256101 (2001).
[20] V. Holy, G. Springholz, M. Pinczolits, and G. Bauer, Phys. Rev. Lett. **83**, 356 (1999).
[21] D. Pan, Y. P. Zeng, J. M. Li, C. H. Zhang, M. Y. Kong, H. M. Wang, C. Y. Wang, and J. Wu, J. Cryst. Growth **175**, 760 (1997).
[22] O. Kienzle, F. Ernst, M. Ruhle, O. G. Schmidt, and K. Eberl, Appl. Phys. Lett. **74**, 269 (1999).
[23] G. Springholz, M. Pinczolits, P. Mayer, V. Holy, and G. Bauer, Phys. Rev. Lett. **84**, 4669 (2000).
[24] V. A. Shchukin, D. Bimberg, V. G. Malyshkin, and N. N. Ledentsov, Phys. Rev. B **57**, 12 262 (1998).
[25] Y. W. Zhang, S. J. Xu, and C.-H. Chiu, Appl. Phys. Lett. **74**, 1089 (1999).
[26] P. Liu, Y. W. Zhang, and C. Lu, Appl. Phys. Lett. **80**, 3910 (2002).